Analysis of helical armature windings with particular reference to superconducting a.c. generators

A.F. Anderson, B.Sc., Ph.D., C.Eng., M.I.E.E., J.R. Bumby, B.Sc., Ph.D., and B.I. Hassall, B.Sc.

Indexing terms: *Generators, Superconductivity*

Abstract: An unusual form of polyphase armature winding is described in which conductors lie on a helix of constant radius as they pass from one end of the machine to the other. There are no end windings. An analysis of the winding is performed which allows analytical expressions for the flux densities and machine reactances to be found. Measured and calculated values of synchronous reactance agree to within 2%. Some of the more unusual properties of helical windings are discussed.

List of symbols

H = magnetic field vector, A/m
H_r = radial component of magnetic field, A/m
H_z = axial component of magnetic field, A/m
H_θ = tangential component of magnetic field, A/m
$\hat{I}$ = peak phase current, A
$I_n(nkr)$ = modified Bessel function of first kind, order n, argument nkr
$I'_n(nkr)$ = (d/dr)($I_n(nkr)$)
$K_n(nkr)$ = modified Bessel function of second kind, order n, argument nkr
$K'_n(nkr)$ = (d/dr)($K_n(nkr)$)
K_θ = tangential component of linear current density, A/m
K_z = axial component of linear current density, A/m
L = self-inductance, H
M = mutual inductance, H
T_{ph} = number of turns in series per phase = $Z/2a$
Z = number of armature conductors per phase
$A_{01}, A_{02}, A_{03}, A_{04}, A_{05}, A_{06}, A_{07}, A_\mu, B_\mu, C_1, C_2, D_n, F_n, \psi_{1\mu}, \psi_{2\mu}, \mu, \nu$ = Constants in general solution of Laplace's equation
Φ = magnetic flux linkage
Ω = magnetic scalar potential
$\beta_n(nkr_i)$ = $K_n(nkr_i)/I_n(nkr_i)$
$\gamma_n(nkr_i)$ = $K'_n(nkr_i)/I'_n(nkr_i)$
a = number of parallel paths per phase
b = number of phasebands per phase
f = system frequency (50 Hz)
k_{wn} = nth harmonic winding factor = $k_{bn}k_{sn}$
k_{bn} = nth harmonic breadth factor
k_{sn} = nth harmonic skew factor
k_{rn} = nth harmonic radial-flux-density environmental screen factor
$k_{\theta n}$ = nth harmonic tangential-flux-density environmental screen factor
k_{zn} = nth harmonic axial-flux-density environmental screen factor
k = $\pi/2l$
l = armature winding half-length, m
m = number of phases
n = space harmonic order
q = time harmonic order
r = radius of magnetic field point, m
r_c = radiation screen radius, m
r_D = outer radius of outer rotor, m
r_f = radius of superconducting field winding, m
r_i = winding radius, m
r_x = environmental screen inner radius, m
x = $(2\pi/m)(i-1), i = 1, 2, \cdots$ m
x_s = synchronous reactance, Ω, p.u.
x'_d = transient reactance, Ω, p.u.
x''_d = subtransient reactance, Ω, p.u.
x''_{dc} = subtransient reactance associated with radiation screen, Ω, p.u.
α = phaseband displacement, rad
$\delta_n(nkr_i)$ = constant = $[K_n(nkr_i) - \gamma_n(nkr_i)I_n(nkr_i)]$
θ = circumferential progression, rad
ρ = resistivity, Ωm
σ = phasespread, rad
μ_0 = permeability of free space, H/m
ω = angular frequency $2\pi f$, rad/s

Suffixes

g = phasegroup
n = space harmonic order
ph = phase
r = radial component
z = axial component
θ = tangential component

1 Introduction

Since 1940 the unit size of two-pole 3000 rev/min turbogenerators has increased from 60 to 660 MW. At the same time, the specific power output has increased from 0·3 kW/kg to 2 kW/kg;[1] in order words, there has been almost a sevenfold improvement in the power/weight ratio. This has been made possible by the introduction of hydrogen cooling and, more recently, water cooling, of the stator conductors, which has enabled more effective use to be made of the iron and copper within the machine.

Within the framework of the maximum magnetic and

Paper 675C, first received 9th October 1979 and in revised form 25th February 1980

Dr. Anderson is with the Electromagnetics Group in the Electrical Research Department of C.A. Parsons Ltd., Newcastle, England; Dr. Bumby is with the Department of Engineering Science, University of Durham, Science Laboratories, South Road, Durham DH1 3LE, England; and Mr. Hassell is with the University of Leeds, England

0143–7046/80/03129 + 16 $01·50/0

electric loadings used today, it appears that there may be difficulties in increasing the size of conventional generators beyond 2000 MW; difficulties which arise because of two limits. These are: first, the limit on maximum indivisible weight which is set by power station cranage and bridge and ship loadings; secondly, the limit on the length between rotor bearings, which is set by the critical speeds.[2] One possible way of overcoming weight limitations would be by subdividing the inner stator, which is usually the heaviest item, and building it on site from smaller factory-built assemblies.[3] Other ways of overcoming, for instance, the problem of rotor length, are by developing slotless windings[4,5] or alternatively, superconducting machines.[6–9] In both cases, higher specific power outputs become possible, albeit at the cost of introducing new technology.

One advantage of either slotless or superconducting generators should be increased efficiency. One of the main reasons why the efficiency of the superconducting generator can be increased[8] is because of the elimination of the rotor excitation loss, which is typically 6 MW for a conventional 1300 MW generator.

The work of the present authors has been confined to the superconducting generator; the essential components of which are shown in Fig. 1. A superconducting rotor winding at 5 K, supported in slots in a stainless-steel rotor forging, is surrounded by an ambient temperature rotor screen to protect the superconductor from transient and negative sequence armature fluxes. The ambient temperature stator consists of two parts: the first is a self-supporting structure in which the water-cooled copper armature is embedded; the second is an iron core, or environmental screen, which screens the environment from magnetic fields and increases the radial flux density and consequently the induced armature e.m.f. per metre length. This paper is concerned with the properties and design of the novel helical stator winding in particular.

Helical windings are not new and found limited favour for dynamos in Germany in the late 1880s[12,13] and have since been revived for small d.c. machines of the ironless type, where they offer the advantage of low inertia and smooth torque at low speeds. They have also been used for linear motors[15] and transverse flux tubular motors.[16] The use in large a.c. machines was first proposed by Ross, Anderson and Macnab[10,11] who suggested it as a suitable armature winding for superconducting a.c. generators. More recently, a 4 MVA helical armature winding has been used by Watanabe *et al.*[17] as the armature winding for use in either a slotless or a superconducting generator, and Conley *et al.*[18] have used a helical winding in an experimental 10 MVA superconducting a.c. generator at MIT.

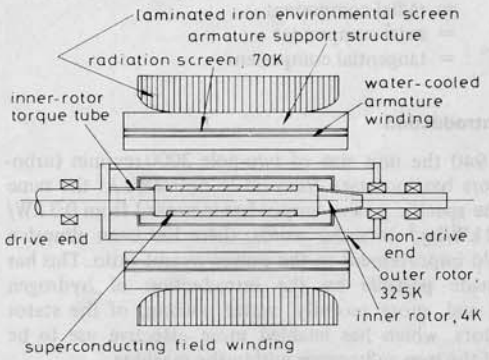

Fig. 1 *Basic components of a.c. superconducting generator*

The helical winding has no distinct division into active and end regions as has the conventional winding, because each conductor follows a helical path of constant pitch from end to end of the machine, see Section 2. In the conventional winding on the other hand, each conductor follows an axial path in the active region and only has a circumferential component to its path in the end regions. Thus the helical winding is characterised by a circumferential component of current density, which only decreases gradually with increasing axial distance from the ends; instead of being confined to the end winding region as in the conventional winding. This suggests that there might be axial flux problems which would not occur with a more conventional winding. However, work by Tavner *et al.*[19] has shown that, contrary to what might be expected, the end-region axial fluxes in the iron core produced by a helical air-gap winding are less than those produced by a corresponding conventional diamond winding. Such observations are also supported by the work of Watanabe *et al.*[17]

The synchronous and subtransient reactances are fundamental to generator design and performance and, in order to design a helical winding, these reactance expressions must be developed in the simplest possible form. In the present paper the magnetic field distributions within the generator which are produced by a helical winding are obtained in terms of Bessel functions and reactance expressions are then derived, which account for all the armature space harmonics. In this way the lowest harmonic sum that gives satisfactory reactances can be used. An alternative to the above method is to use a transmission-line analogue.[20] However, although this method yields magnetic field values without the introduction of Bessel functions, the solution is numerical. This is a disadvantage of the method, since analytic inductance expressions simplify iterative generator design techniques.[8] More recently, Alwash[28] has developed an analytic 3-dimensional method which is expressed in Fourier-Bessel expansions. The solution requires extensive computation for the boundary matchings, although it is capable of achieving high accuracy.

2 Development of an helical armature winding

As generator sizes increase, the length between bearings becomes a limitation, see Section 1. Increased output in larger machines can only be obtained by increasing the output per unit length by an amount which keeps the length between bearings down to an acceptable level. In the case of the conventional machine, electric and magnetic loadings can only be increased marginally and therefore the only remaining variable is the effective stator-winding diameter. Stator-winding diameter is however closely tied to the rotor diameter because of the need to closely couple the two windings and so give an acceptable rotor m.m.f. and stator magnetic loading. Thus since the rotor diameter is limited by rotational stresses, so too indirectly is the stator diameter.

On the other hand such restrictions no longer apply to the superconducting machine, and a considerable decoupling between rotor and stator windings becomes possible without incurring the same penalties that would arise in the conventional machine. This is because the superconducting winding can operate at current densities at least ten times greater than is current turbogenerator practice and this, in turn, permits magnetic loadings at least as high as those obtained in the conventional machine, i.e. 0·9 T, but at a

substantially increased stator diameter; even though the rotor diameter is still limited by rotational stresses to a value not far different from current practice. Hence the stator diameter can be increased from 1·6 m in the conventional machine to 2·0 m in the superconducting machine, with a consequent increase in the possible output per metre. Furthermore, in the conventional turbogenerator the available winding space is limited by the need to support the windings in slots in the iron core, whereas in the case of the airgap-wound superconducting machine the proportion of the circumference available for the winding increases, as does the possible winding depth; this allows the electric loading to increase from typically 200 kA/m to 300 kA/m in a 1300 MW design. The increased armature-winding diameter and electric loading combine in the case of the superconducing generator to produce a short, large-diameter armature winding with a power output of 300 MW/m instead of the 100 MW/m typical for the conventional turbogenerator.

A secondary result of the absence of clearly defined closed magnetic circuits to constrain the flux is that the distinction between active and end regions becomes blurred.

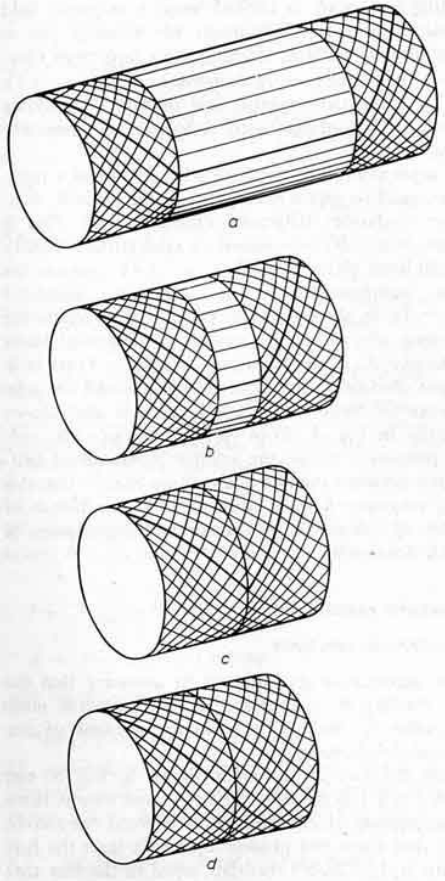

Fig. 2 *Evolution of helical winding from diamond lap winding*

a Diamond lap winding, long machine
b Diamond winding, short machine with greater specific machine output
c Diamond winding, with straight portion removed to give semi-helical winding
d Full helical winding

Because of the way in which the active and end regions merge, it becomes apparent at a fairly early stage in the design that the conventional winding might not necessarily be the best and that alternatives should be examined. If a helical winding is used, then it can be uniformly supported from end to end; a feature which is particularly important now that the armature conductors are no longer shielded from the main flux by the stator teeth and must therefore bear the full machine forces.

To understand how a helical winding works, consider the winding length of a diamond winding to be progressively reduced, as in Fig. 2, by eliminating the so-called central active region and allowing the two diamond-end windings to coalesce and form a helical winding. One phase of a two-pole helical winding is shown in Fig. 3, where each phase consists of two parallel-connected helical loops, each of which is termed a phase group. Each phase group consists of one right-hand (inner) helical phaseband connected in series with a returning left-hand (outer) helical phaseband; a right hand phaseband being defined as that which traces a right hand screw.

Because the development of large generators in the UK is generally concerned with two-pole 3000 rev/min^2 machines, only two-pole helical windings are considered in the present paper.

3 Method of analysis

3.1 *Notation adopted in the description of a helical winding*

Each phaseband is described by three parameters:

(*a*) + 1 or − 1 depending on whether a right-hand (r.h.) or left-hand (l.h.) helixed phaseband is considered

(*b*) the circumferential angular position α at which the centre of the phaseband crosses $z = 0$, Fig. 3

(*c*) the radius of the phaseband r_i.

e.g. $K_z(r_i, \alpha, +1)$ refers to the axial component of linear current density for the ith right-hand phaseband centred at angular position α and radius r_i.

The angular position of the two phasebands in a phase-group are related as

$$\alpha_i(-1) = \alpha_i(+1) + \pi \tag{1}$$

while the angular position of a phasegroup is defined as the angular position of its right-hand phaseband,

$$\alpha_g = \alpha(+1) \tag{2}$$

and the angular position of a phase as

$$\alpha_{ph} = \alpha_g$$

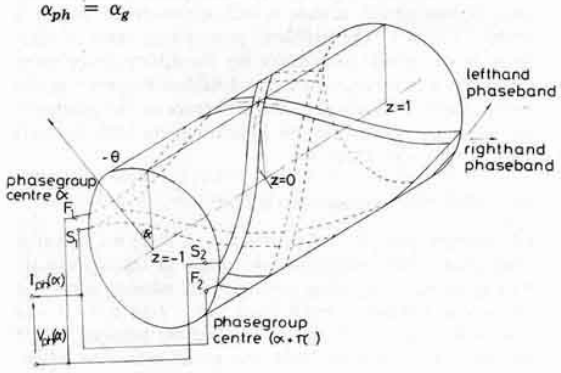

Fig. 3 *One phase of helical winding*

or

$$\alpha_{ph} = \alpha_g + \pi \tag{3}$$

because the complete phase is symmetrical.

3.2 Representation of a helical winding

Each phaseband of the helical armature winding is represented by a linear current density sheet of negligible radial thickness, with axial and tangential linear current-density components as described in Section 11.1. In order to yield a closed analytical solution to Laplace's equation, a periodic variation is introduced in the axial direction in a similar manner to that suggested by Hammond,[21] by assuming the helical winding to be one of an infinite number of helical windings placed end to end. Such a winding is termed an 'infinite periodic helical winding'.

3.3 Representation of the environmental screen

A superconducting a.c. generator requires an environmental screen which is normally constructed from laminated magnetic iron, in order to screen the environment from the magnetic fields produced inside the generator. However, conducting environmental screens have been suggested,[6] particularly for airborne applications,[22] and this analysis contains solutions for both types of screen. The general effect of the iron environmental screen is, as expected, to enhance the main magnetic field, whereas the conducting screen has a demagnetising effect.

The environmental screen is assumed to be infinitely long in the axial direction. If it is constructed from laminated magnetic iron it is assumed to have infinite permeability and zero conductivity, i.e. there are no eddy currents. If on the other hand it is constructed from non-magnetic conducting material, it is assumed to have a relative permeability of unity and infinite conductivity. In either case the effect of the screen is included in the magnetic-field analysis by using an image winding with the appropriate current polarity placed outside the actual helical winding. In the case of the iron environmental screen, the image winding assists the radial field and therefore is of the same polarity as the armature winding. In the case of a conducting screen, the image winding must oppose the radial field and therefore is of opposite polarity to the armature winding.

In practice, the iron environmental screen tends to be shorter than the helical armature winding, as indicated in Fig. 1, and it is likely too that a conducting end screen would be used. Consequently the assumption of an infinitely long environmental screen, whilst necessary to enable a ready solution to the problem, gives a high value of reactance and is mainly responsible for the difference between calculated and measured reactance values. However, in the model results of Section 6, the difference in the synchronous reactance is less than 2%, indicating how little the ends contribute to the reactance.

3.4 Mathematical solution method

The infinite periodic helical winding is analysed in cylindrical polar co-ordinates with the origin of the co-ordinate system taken at the axial centre of the winding such that the actual winding extends from $z = +l$ to $z = -l$ and constitutes one half-period of the 'infinite periodic helical winding'. The magnetic field due to an individual phaseband at the general circumferential position α_i is obtained from a solution of Laplace's equation, expressed in terms of magnetic scalar potential, by the method of separation of variables. Magnetic scalar potential terms produced by the image winding which represents the environmental screen are combined with those from the helical armature winding and magnetic-field distributions are then obtained in the manner described in Section 11.2.

4 Magnetic field of a helical winding

The magnetic field distributions for an individual phaseband of an infinite periodic helical winding with an environmental screen are shown in Table 1. The environmental screen modifies the magnetic field distributions of the unscreened winding by the geometric factors defined in Table 2.

The magnetic field distributions described in Table 1 include terms that are independent of axial or tangential position. The effect of these zero-order terms is reflected in the magnetic field distributions as a solenoidal field which is produced by the zero-order component in the tangential linear current density $K_\theta(r_i, \alpha_i, \pm 1)$. Because the winding is part of an infinite helix, a magnetic field component is produced only inside the winding, just as though it were an infinite solenoid. The zero-order component of axial linear current density, $K_z(r_i, \alpha_i, \pm 1)$, produces a tangential magnetic field outside the winding that varies, in accordance with Ampere's law, inversely with radius.

Using superposition to combine a left-hand and a right-hand phaseband to give a phasegroup, as in Table 3, eliminates the zero-order tangential magnetic field. This is because the zero-order component of axial current density in the right-hand phaseband, $K_z(r_i, \alpha_i, +1)$, opposes the equivalent component in the left-hand phaseband $K_z(r_i, \alpha_i, -1)$, as shown in Fig. 4. However, because the corresponding zero-order components of tangential linear current density, $K_\theta(r_i, \alpha_i, +1)$ and $K_\theta(r_i, \alpha_i, -1)$ are both in the same direction their effect is additive and the solenoidal magnetic field is increased. This is also shown schematically in Fig. 4. When two phasegroups are combined to produce a phase, the relative phaseshift of 180° which exists between the two phasegroups ensures that this solenoidal magnetic field is eliminated. The influence of this effect on measured and computed inductances is described in Section 6.

5 Reactance calculations

5.1 Synchronous reactance

Reactance expressions are obtained by assuming that the armature winding is concentrated at the geometric mean winding radius r_s, and by only taking account of the fundamental time harmonic.

Consider the two helical loops shown in Fig. 5; one centred at $\theta = 0$ and the other at $\theta = \alpha$, and assume there to be a phasegroup of Z/b turns centred about the second loop. The flux from this phasegroup which links the first helical turn is, by Gauss's theorem, equal to the flux that crosses normally any surface bounded by the first, like that shown in Fig. 5. Evaluating the resulting surface integrals as described in Section 11.4 allows the inductance between phasegroups to be expressed as in eqn. 51. If the phasegroup inductance values are combined appropriately, phase and generator inductances are obtained, see eqns. 53 and

Table 1: Magnetic field distributions produced by a helical phaseband

Linear current-density distributions

$$K_z[r_i, \alpha_i, \pm 1] = \pm \frac{Zi_{phq}}{2\pi abr_i} \pm \frac{Zi_{phq}}{\pi abr_i} \sum_{n=1}^{\infty} k_{bn} \cos n(\theta - \alpha_i \mp kz)$$

$$K_\theta[r_i, \alpha_i, \pm 1] = \frac{Zi_{phq}}{4lab} + \frac{Zi_{phq}}{2lab} \sum_{n=1}^{\infty} k_{bn} \cos n(\theta - \alpha_i \mp kz)$$

Inside the winding $r \leqslant r_i$

$$\Omega[r_i, \alpha_i, \pm 1] = -\frac{Zi_{phq}z}{4abl} \mp \frac{Zi_{phq}}{\pi ab} \sum_{n=1}^{\infty} \frac{k_{bn}}{n} \frac{k_{\theta n}\gamma_n(nkr_i) I_n(nkr)}{\delta_n(nkr_i)} \sin n(\theta - \alpha_i \mp kz)$$

$$H_r[r_i, \alpha_i, \pm 1] = \mp \frac{Zi_{phq}}{\pi ab} \sum_{n=1}^{\infty} \frac{k_{bn}k_{rn}\gamma_n(nkr_i)\left[-kI_{n-1}(nkr) + \dfrac{I_n(nkr)}{r}\right]}{\delta_n(nkr_i)} \sin n(\theta - \alpha_i \mp kz)$$

$$H_\theta[r_i, \alpha_i, \pm 1] = \pm \frac{Zi_{phq}}{\pi ab} \sum_{n=1}^{\infty} \frac{k_{bn}k_{\theta n}\gamma_n(nkr_i)}{\delta_n(nkr_i)} \frac{I_n(nkr)}{r} \cos n(\theta - \alpha_i \mp kz)$$

$$H_z[r_i, \alpha_i, \pm 1] = +\frac{Zi_{phq}}{4abl} - \frac{Zi_{phq}}{2lab} \sum_{n=1}^{\infty} \frac{k_{bn}k_{zn}\gamma_n(nkr_i) I_n(nkr)}{\delta_n(nkr_i)} \cos n(\theta - \alpha_i \mp kz)$$

Outside the winding $r_i \leqslant r \leqslant r_x$

$$\Omega[r_i, \alpha_i, \pm 1] = \mp \frac{Zi_{phq}\theta}{2ab\pi} \mp \frac{Zi_{phq}}{\pi ab} \sum_{n=1}^{\infty} \frac{k_{bn}}{n} \frac{k_{\theta n}K_n(nkr)}{\delta_n(nkr_i)} \sin n(\theta - \alpha_i \mp kz)$$

$$H_r[r_i, \alpha_i, \pm 1] = \mp \frac{Zi_{phq}}{\pi ab} \sum_{n=1}^{\infty} \frac{k_{bn}k_{rn}\left[kK_{n-1}(nkr) + \dfrac{K_n(nkr)}{r}\right]}{\delta_n(nkr_i)} \sin n(\theta - \alpha_i \mp kz)$$

$$H_\theta[r_i, \alpha_i, \pm 1] = \pm \frac{Zi_{phq}}{2\pi abr} \pm \frac{Zi_{phq}}{\pi ab} \sum_{n=1}^{\infty} \frac{k_{bn}k_{\theta n}}{\delta_n(nkr_i)} \frac{K_n(nkr)}{r} \cos n(\theta - \alpha_i \mp kz)$$

$$H_z[r_i, \alpha_i, \pm 1] = -\frac{Zi_{phq}}{2lab} \sum_{n=1}^{\infty} \frac{k_{bn}k_{zn}K_n(nkr)}{\delta_n(nkr_i)} \cos n(\theta - \alpha_i \mp kz)$$

Environmental screen factors k_{rn}, $k_{\theta n}$, k_{zn} defined in Table 2
$\delta_n(nkr_i) = [K_n(nkr_i) - \gamma_n(nkr_i) I_n(nkr_i)]$

55. The synchronous reactance of a helical winding, given in eqn. 55, can be expressed in the more usual form as

$$x_{sn} = \frac{m}{\pi n} \omega\mu_0 T_{ph}^2 k_{wn}^2 k_{rn} 2l \text{ ohms.}$$

$$n = 2\tau m \pm 1, \tau \text{ any integer} \tag{4}$$

with the winding factor

$$k_{wn}^2 = k_{sn}^2 k_{bn}^2 \tag{5}$$

k_{sn}^2 is the skew factor defined by eqn. 48 and k_{rn} the nth harmonic radial flux environmental screen enhancement factor defined in the first column of Table 2.

5.2 Subtransient and transient reactance

Under fault conditions the armature flux is initially deflected around the outside of the outer rotor, as if this outer rotor were a perfectly conducting screen. This effect is included in the analysis by representing the outer rotor screen by an image winding at the surface of the outer rotor, which is equal in magnitude, but opposite in phase, to the armature current. This current introduces an additional magnetic scalar potential term into the magnetic field solution as described in Section 11.4.4, such that the resulting integration over the Gaussian surface of Fig. 5 gives for the subtransient reactance:

$$x''_{dn} = \frac{m}{\pi n} \omega\mu_0 T_{ph}^2 k_{wn}^2 k_{rn} 2l \frac{\left[1 - \dfrac{\gamma_n(nkr_s)}{\gamma_n(nkr_D)}\right]}{\left[1 - \dfrac{\beta_n(nkr_x)}{\gamma_n(nkr_D)}\right]} \text{ ohms} \tag{6}$$

where the factors $\gamma_n(nkr)$ and $\beta_n(nkr)$ are defined in eqns. 43f and 44b, respectively. This expression is similar to that for the synchronous reactance except for the geometric modifying factors, both of which depend, through Bessel functions, on the armature length. The two modifying factors relate to the different generator components as

$$\left[1 - \frac{\gamma_n(nkr_s)}{\gamma_n(nkr_D)}\right]$$

a geometric factor relating armature and outer rotor

$$\left[1 - \frac{\beta_n(nkr_x)}{\gamma_n(nkr_D)}\right]$$

a geometric factor relating the iron environmental screen and the outer rotor.

(Note: For a conducting environmental screen $\gamma_n(nkr_x)$ replaces $\beta_n(nkr_x)$. Table 4 details all the permutations).

As the fault period progresses flux will penetrate the outer rotor and two further reactance expressions require definition; the first being associated with the radiation screen, when flux is deflected round the outside of this screen, and the second, the transient reactance, when flux is deflected round the outside of the rotor field winding. These can be obtained from eqn. 6 by substituting the outer rotor radius r_D, by the radiation screen radius r_c, and the superconducting field winding radius r_f, respectively. The transient reactance is unusual in the superconducting generator because it is associated with a transient open-circuit time constant greater than 100 s compared with one of less than 10 s in the conventional turbogenerator.

5.3 *Effect of harmonics on reactance calculation*

The reactance between phases and the synchronous reactance are computed for the 1300 MW design of Table 5. This generator has a six-phase armature winding with opposite phasegroups connected in parallel. The results of the reactance calculations are shown in Table 6 first for the fundamental harmonic only and secondly for the harmonic sum of $n = 1$ to 50.

The Table shows that when considering a phase or phasegroup, the space harmonics form an important constituent of the reactance and consequently must be taken into account. However, once all three phases are combined to give the three-phase synchronous magnetising reactance, eqn. 4, many of the space harmonic terms cancel out and only those terms with $n = 2\tau m \pm 1$ are left to contribute to the reactance. The effect of individual harmonics is reflected into any reactance expression through both the skew and environmental screen factors but, more dominantly, by the factor k_{bn}^2, k_{bn} being the breadth factor.

For a six-phase winding, with 30° phase spread, harmonics introduced are the 11th, 13th, 23rd, 25th etc., for which the variation of k_{bn}^2/n is shown in Table 7. The first harmonic is dominant such that the synchronous reactance calculated with $n = 1$ shows negligible error when compared with the value calculated using the harmonic sum.

The variation of k_{bn}^2/n for the three-phase winding with a phase spread of 60° is also shown in Table 7, the harmonics now being 5th, 7th, 11th, 13th etc.. Again, the first harmonic is dominant, indicating that in calculating synchronous, subtransient and transient reactance, only first-harmonic terms need be considered.

Table 2: Expressions for *n*th space harmonic environmental screen factor

			Inside stator $r \leqslant r_s$	Outside stator $r_s \leqslant r \leqslant r_x$
infinite straight winding	Iron environmental screen	k_{rn}	$\left\{1 + \left(\frac{r_s}{r_x}\right)^{2n}\right\}$	$\left\{1 + \left(\frac{r}{r_x}\right)^{2n}\right\}$
		$k_{\theta n}$	$\left\{1 + \left(\frac{r_s}{r_x}\right)^{2n}\right\}$	$\left\{1 - \left(\frac{r}{r_x}\right)^{2n}\right\}$
	Conducting environmental screen	k_{rn}	$\left\{1 - \left(\frac{r_s}{r_x}\right)^{2n}\right\}$	$\left\{1 - \left(\frac{r}{r_x}\right)^{2n}\right\}$
		$k_{\theta n}$	$\left\{1 - \left(\frac{r_s}{r_x}\right)^{2n}\right\}$	$\left\{1 + \left(\frac{r}{r_x}\right)^{2n}\right\}$
periodic helical winding	Iron environmental screen	k_{rn}	$\left\{1 - \frac{\beta_n(nkr_x)}{\gamma_n(nkr_s)}\right\}$	$\left\{1 - \frac{\beta_n(nkr_x)}{\gamma_n(nkr)}\right\}$
		$k_{\theta n}, k_{zn}$	$\left\{1 - \frac{\beta_n(nkr_x)}{\gamma_n(nkr_s)}\right\}$	$\left\{1 - \frac{\beta_n(nkr_x)}{\beta_n(nkr)}\right\}$
	Conducting environmental screen	k_{rn}	$\left\{1 - \frac{\gamma_n(nkr_x)}{\gamma_n(nkr_s)}\right\}$	$\left\{1 - \frac{\gamma_n(nkr_x)}{\gamma_n(nkr)}\right\}$
		$k_{\theta n}, k_{zn}$	$\left\{1 - \frac{\gamma_n(nkr_x)}{\gamma_n(nkr_s)}\right\}$	$\left\{1 - \frac{\gamma_n(nkr_x)}{\beta_n(nkr)}\right\}$

If no environmental screen $k_{rn}, k_{\theta n}, k_{zn} = 1$
$\gamma_n(nkr)$ always negative
$\beta_n(nkr)$ always positive

5.4 *Comparison of reactance of a helical winding with those of a straight winding*

By assuming the armature winding to be infinitely long and each phase to be represented by a current sheet of the form

$$\frac{2T_{ph}k_{wn}i_{ph}}{\pi r_s}\sin n\theta \text{ A/m} \tag{7}$$

the synchronous reactance is

$$x_{sn} = \frac{m}{\pi n}\omega\mu_0 T_{ph}^2 k_{wn}^2 k_{rn} 2l \text{ ohms} \tag{8}$$

where k_{wn}, the winding factor is

$$k_{wn} = k_{bn}k_{pn} \tag{9}$$

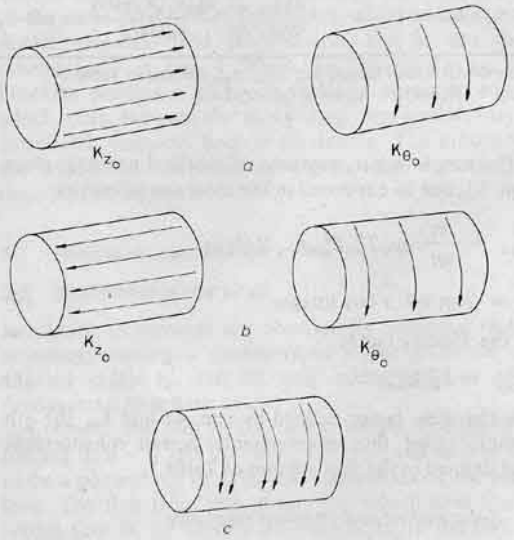

Fig. 4 *Zero-order components of phaseband and phasegroup linear current-density distributions*

a Zero-order components of right-hand phaseband
b Zero-order components of left-hand phaseband
c Zero-order components of phasegroup

Table 3: Magnetic field distributions produced by a helical phasegroup

Linear current density distributions

$$K_{zg}[r_i, \alpha_i] = \frac{2Zi_{phq}}{\pi abr_i} \sum_{\substack{n=1 \\ n \text{ odd}}}^{\infty} k_{bn} \cos n(\theta - \alpha_i) \cos nkz + \frac{2Zi_{phq}}{\pi abr_i} \sum_{\substack{n=2 \\ n \text{ even}}}^{\infty} k_{bn} \sin n(\theta - \alpha_i) \sin nkz$$

$$K_{\theta g}[r_i, \alpha_i] = \frac{Zi_{phq}}{2lab} + \frac{Zi_{phq}}{lab} \sum_{\substack{n=1 \\ n \text{ odd}}}^{\infty} k_{bn} \sin n(\theta - \alpha_i) \sin nkz + \frac{Zi_{phq}}{lab} \sum_{\substack{n=2 \\ n \text{ even}}}^{\infty} k_{bn} \cos n(\theta - \alpha_i) \cos nkz$$

Inside the winding $r \leqslant r_i$

$$\Omega_g[r_i, \alpha_i] = -\frac{Zi_{phq} \cdot z}{2lab} + \frac{2Zi_{phq}}{\pi ab} \sum_{n=1}^{\infty} \frac{k_{bn}}{n} \frac{k_{\theta n}\gamma_n(nkr_i) I_n(nkr)}{\delta_n(nkr_i)} \begin{cases} -\cos nkz \sin n(\theta - \alpha_i) & n \text{ odd} \\ \sin nkz \cos n(\theta - \alpha_i) & n \text{ even} \end{cases}$$

$$H_{rg}[r_i, \alpha_i] = -\frac{2Zi_{phq}}{\pi ab} \sum_{n=1}^{\infty} \frac{k_{bn}k_{rn}\gamma_n(nkr_i) \left[-kI_{n-1}(nkr) + \frac{I_n(nkr)}{r} \right]}{\delta_n(nkr_i)} \begin{cases} -\cos nkz \sin n(\theta - \alpha_i) & n \text{ odd} \\ \sin nkz \cos n(\theta - \alpha_i) & n \text{ even} \end{cases}$$

$$H_{\theta g}[r_i, \alpha_i] = +\frac{2Zi_{phq}}{\pi ab} \sum_{n=1}^{\infty} \frac{k_{bn}k_{\theta n}\gamma_n(nkr_i)}{\delta_n(nkr_i)} \frac{I_n(nkr)}{r} \begin{cases} \cos nkz \cos n(\theta - \alpha_i) & n \text{ odd} \\ \sin nkz \sin n(\theta - \alpha_i) & n \text{ even} \end{cases}$$

$$H_{zg}[r_i, \alpha_i] = \frac{Zi_{phq}}{2lab} - \frac{Zi_{phq}}{lab} \sum_{n=1}^{\infty} \frac{k_{bn}k_{zn}\gamma_n(nkr_i) I_n(nkr)}{\delta_n(nkr_i)} \begin{cases} \sin nkz \sin n(\theta - \alpha_i) & n \text{ odd} \\ \cos nkz \cos n(\theta - \alpha_i) & n \text{ even} \end{cases}$$

Outside the winding $r_i \leqslant r \leqslant r_x$

$$\Omega_g[r_i, \alpha_i] = +\frac{2Zi_{phq}}{\pi ab} \sum_{n=1}^{\infty} \frac{k_{bn}}{n} \frac{k_{\theta n}K_n(nkr)}{\delta_n(nkr_i)} \begin{cases} -\cos nkz \sin n(\theta - \alpha_i) & n \text{ odd} \\ \sin nkz \cos n(\theta - \alpha_i) & n \text{ even} \end{cases}$$

$$H_{rg}[r_i, \alpha_i] = -\frac{2Zi_{phq}}{\pi ab} \sum_{n=1}^{\infty} \frac{k_{bn}k_{rn} \left[kK_{n-1}(nkr) + \frac{K_n(nkr)}{r} \right]}{\delta_n(nkr_i)} \begin{cases} -\cos nkz \cos n(\theta - \alpha_i) & n \text{ odd} \\ \sin nkz \sin n(\theta - \alpha_i) & n \text{ even} \end{cases}$$

$$H_{\theta g}[r_i, \alpha_i] = +\frac{2Zi_{phq}}{\pi ab} \sum_{n=1}^{\infty} \frac{k_{bn}k_{\theta n}}{\delta_n(nkr_i)} \frac{K_n(nkr)}{r} \begin{cases} \cos nkz \cos n(\theta - \alpha_i) & n \text{ odd} \\ \sin nkz \sin n(\theta - \alpha_i) & n \text{ even} \end{cases}$$

$$H_{zg}[r_i, \alpha_i] = -\frac{Zi_{phq}}{lab} \sum_{n=1}^{\infty} \frac{k_{bn}k_{zn}K_n(nkr)}{\delta_n(nkr_i)} \begin{cases} \sin nkz \sin n(\theta - \alpha_i) & n \text{ odd} \\ \cos nkz \cos n(\theta - \alpha_i) & n \text{ even} \end{cases}$$

Environmental screen factors $k_{rn}, k_{\theta n}, k_{zn}$ defined in Table 2
$\delta_n(nkr_i) = [K_n(nkr_i) - \gamma_n(nkr_i) I_n(nkr_i)]$

Table 4: Expressions for the *n*th space harmonic combined environmental and rotor screen factors

	Inside stator $r_D < r < r_s$	Outside stator $r_s < r < r_x$
k'_{rn}	$\left[1 + \frac{a}{\gamma_n(nkr_s)}\right] \frac{\left[1 + \frac{\gamma_n(nkr)}{b}\right]}{\left[1 - \frac{a}{b}\right]}$	$\left[1 - \frac{a}{\gamma_n(nkr)}\right] \frac{\left[1 - \frac{\gamma_n(nkr_s)}{b}\right]}{\left[1 - \frac{a}{b}\right]}$
$k'_{\theta n}, k'_{zn}$	$\left[1 - \frac{a}{\gamma_n(nkr_s)}\right] \frac{\left[1 - \frac{\beta_n(nkr)}{b}\right]}{\left[1 - \frac{a}{b}\right]}$	$\left[1 - \frac{a}{\beta_n(nkr)}\right] \frac{\left[1 - \frac{\gamma_n(nkr_s)}{b}\right]}{\left[1 - \frac{a}{b}\right]}$

$a = \beta_n(nkr_x)$ for iron environmental screen
$a = \gamma_n(nkr_x)$ for conducting environmental screen
$a = 0$ for no environmental screen
$b = \beta_n(nkr_D)$ for iron rotor screen
$b = \gamma_n(nkr_D)$ for conducting rotor screen
$b = 0$ for no rotor screen

k_{pn} being the nth harmonic pitch factor. This equation is of the same form as that for a helical winding, eqn. 4, except for the winding factor, k_{wn}, and environmental screen factor k_{rn}. The environmental screen factors obtained by the two dimensional analysis outlined above, see References 23, 24 and 6, are shown in Table 2 along with the corresponding values for the helical winding, the fundamental difference between the environmental screen factors being the dependence on winding length introduced by the helical winding. However, finite-length effects become less prominent as the length/diameter ratio of the helical winding increases. Hence, as this ratio tends to infinity (i.e. as the winding length tends to infinity) the environmental screen factors for the helical winding tend to become the same as those for a long straight winding. In the same way, the modifying factors associated with the subtransient reactance of the helical winding, defined in eqn. 6, tend to

$$\frac{\left[1 \pm \left(\frac{r_s}{r_x}\right)^{2n}\right]\left[1 - \left(\frac{r_D}{r_s}\right)^{2n}\right]}{\left[1 \pm \left(\frac{r_D}{r_x}\right)^{2n}\right]}$$

$\left.\begin{matrix}+\\-\end{matrix}\right\}$ iron environmental screen
conducting environmental screen

as the winding length tends to infinity. This is identical with the expression obtained for the long straight winding with a conducting environmental screen by Appleton and Anderson[6] and an iron environmental screen by Miller and Hughes.[25]

Unlike the environmental screen factors, which tend to the same value as winding length increases, the skew factor, k_{sn}^2, of the helical winding does not tend to 1 as the armature length tends to infinity, but to 0·5. This arises because, whatever the length of the generator, a proportion of the flux must be lost due to skewing of the conductors through 180° over the total generator length. The variation of skew factor k_{sn}^2 with length/diameter ratio is shown in Fig. 6.

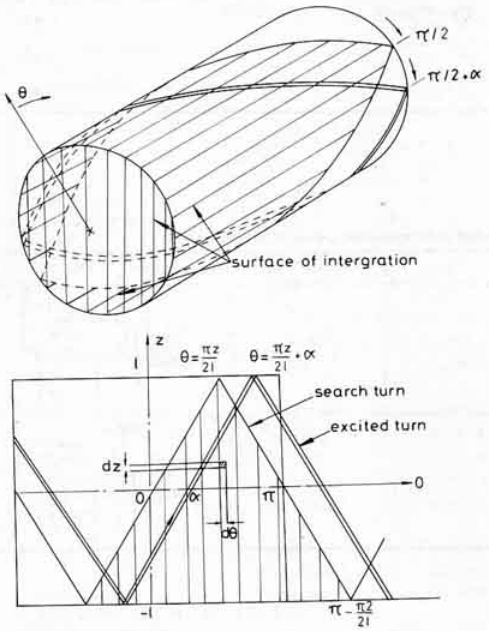

Fig. 5 *Surface of integration for calculation of inductance*

One effect of skewing the armature conductors is to reduce the amount of rotor flux linking the armature winding, and consequently the induced e.m.f.. However, as the rotor flux density at the armature winding falls off towards the ends of the machine, the majority of the generated e.m.f. is towards the centre of the machine. Hence in practical designs this loss of flux is found to be less than 10%.

This loss of flux in the helical winding is compensated for by the superior winding support and by the reduction of synchronous reactance (and in consequence the reduced armature reaction). This drop in synchronous reactance arises because the skew factor for a helical winding is less than unity and because the environmental screen factor k_{rn} is also less than it would be for a straight winding. k_{rn} has a value of 1·54 for a straight winding and 1·38 for the helical winding design of Table 5.

6 Comparison of inductance calculations with model results

To assess the accuracy of the inductance expressions of

Table 5: 1300 MW a.c. generator design parameters

Parameter	Value
MVA rating	1530 MVA
Power factor	0·85 lagging
Terminal voltage (r.m.s./phase)	16 kV
Armature current (r.m.s./phase)	15·94 kA
No. phases	6
No. parallel paths/phase	2
No. phasebands/phasegroup	2
No. phasegroups/phase	2
No. conductors/phase	48
Field-winding radius	0·423 m
Radiation-screen radius	0·5 m
Outer-rotor inner radius	0·515 m
Outer-rotor outer radius	0·65 m
Armature mean winding radius	1·03 m
Inner radius of iron environmental screen	1·4 m
Armature half-length	2·9 m

Table 6: Calculated reactance values for helical winding with iron environmental screen, showing effect of space harmonics

Harmonic Sum	Reactance p.u. wL_{ph}	$wM_{ph}(\pi/6)$	$wM_{ph}(\pi/3)$	x_s
n = 1 to 50	0·224	0·128	0·056	0·5018
n = 1	0·167	0·145	0·084	0·5013

Table 7: Effect of harmonics on the breadth factor of 6-phase and 3-phase windings

6-phase		3-phase	
n	k_{bn}^2/n	n	k_{bn}^2/n
1	0·97736	1	0·91289
11	0·00073	5	0·00730
13	0·00044	7	0·00266
23	0·00008	11	0·00069

Section 5.1, extensive measurements have been made using a 1:9 scale model of a 1300 MW turbogenerator[26, 28] at Leeds University. The helical winding model has a mean radius of 105 mm and length of 406 mm and is shown in Fig. 7. To simplify construction, it employs comparatively few conductors, 24 per layer, which are disposed in three phases with opposite phasegroups connected in series to minimise errors due to circulating currents. The inductance between individual turns can be measured. The iron environmental screen model, shown in Fig. 8, is manufactured from laminated iron and has an inner radius of 134·5 mm and length of 356 mm. The ends of the environmental screen are manufactured from aluminium with an inner radius of 150 mm and extended 88 mm to the aluminium end plates of the model. The relevant dimensions of the model are summarised in Table 8.

Measured and computed values of interturn mutual inductance, both for the helical winding in air and inside the iron environmental screen, are shown as a function of coil separation in Figs. 9 and 10, respectively. Computed inductance values are obtained by assuming a phasespread of 15° (the total spread of each conductor) and summing to a harmonic order of 81; this being the maximum order accomodated by the computation.

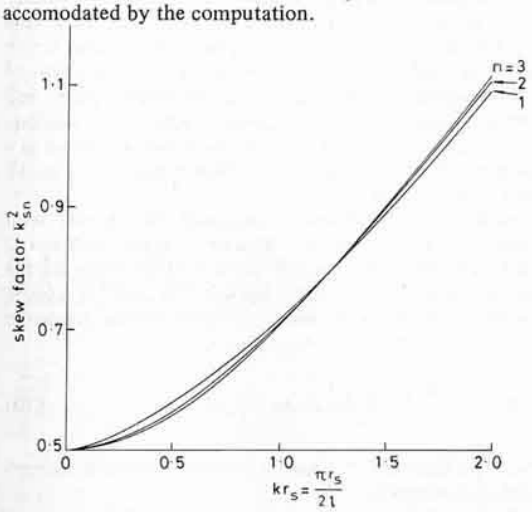

Fig. 6 *Graph of skew factor k_{sn}^2 against kr_s for helical winding*

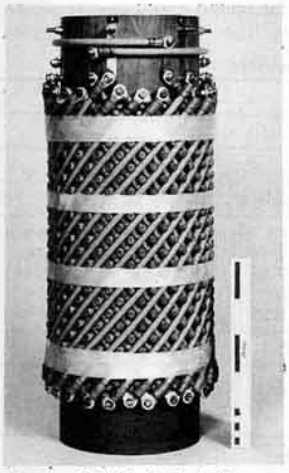

Fig. 7 *Model helical winding*

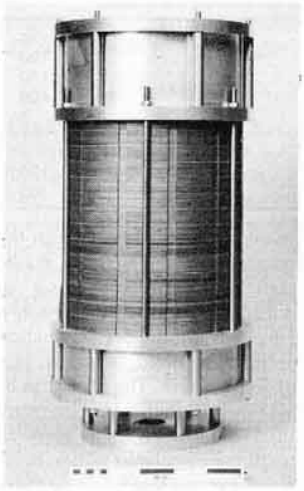

Fig. 8 *Iron environmental screen*

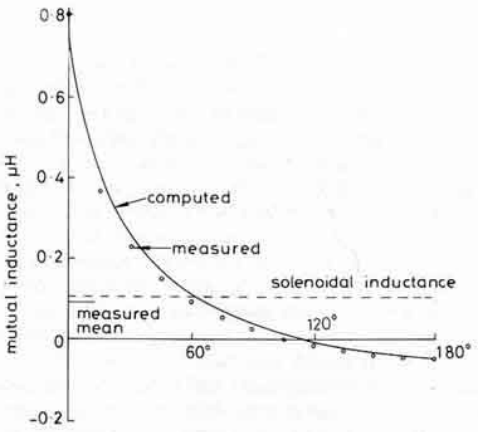

Fig. 9 *Interturn mutual inductance as function of separation for model winding in air*

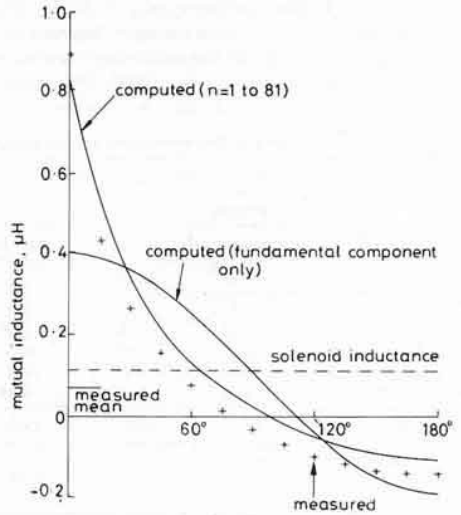

Fig. 10 *Interturn mutual inductance as a function of separation for model helical winding inside iron environmental screen*

Table 8: Model helical winding dimensions

	mm
Helical winding:	
l.h.-layer radius	100
r.h.-layer radius	110
winding length	406
conductor diameter	7
Iron Core:	
inner radius	134·5
length	356

The presence of the 'solenoidal' inductance term in the phasegroup inductances, and interturn inductances, makes comparison of measured and computed phasegroup, or interturn, inductance values difficult because the solenoidal inductance value computed by the 'infinite periodic helical winding' is that of an infinite solenoid, whereas that measured is of a solenoid of finite length. The latter can be substantially different from the former. The interturn mutual inductances measured in air (Fig. 9), however, show very close agreement with the calculated values, being on average higher by 10% of the solenoidal inductance term. These results suggest that the inevitable overestimation of solenoidal inductance has been countered by main flux linkage around the winding ends. When measured in the laminated iron core (Fig. 10) a more pronounced discrepancy, on average 50% of the solenoidal inductance, is shown. This arises because the model core is shorter than the winding and the boundary extended to the machine end plates by aluminium rings of inner radius 150 mm. Consequently, any measured results may be expected to be less than those predicted by the infinite periodic model with the infinitely long environmental screen assumption. Also shown in Fig. 10 is an interturn inductance computation using the fundamental harmonic component only. This clearly demonstrates the high space harmonic content of interturn, or equally phasegroup, mutual inductances.

A comparison of self-inductances is shown in Table 9 and gives two measured and two calculated values of inductance for the winding in air and inside the laminated iron core. The first column gives directly measured values, whilst the second gives values derived from measurements on the previous subgroup. For example, the phase self-inductance was derived from the measurements on 60° spread phasegroups, showing a discrepancy of 2·5% with the directly measured value. This discrepancy, absent from mutual values, is attributable to the conductor necessary to form the series connection spanning 180°. The prominence of this effect is because of the air-cored nature of the geometry, even in the iron core, and exaggerated in the model by the small number of conductors, 16, that form a phase. The computed values of self-inductance depend on conductor size. The first column in Table 9 assumes a full spread for the current sheet of 15° per turn, whereas in the second column a spread of 7·5° has been used. The true angle subtended by the conductor is approximately 3°, but if this spread is used with infinitesimal depth then excessively high inductance values result. In other words if a continuous current sheet is used to represent discrete conductors, a fair model results.

The error between computed and measured values in Table 9 is in all cases less than 10% and the synchronous reactance values agree to within 2%. The final row of Table 9 uses only the fundamental component in eqn. 4 to compute synchronous reactance and gives results to within 2%; indicating that only the fundamental component need be considered when computing synchronous and subtransient reactances.

7 Design of a helical armature winding for use in a superconducting a.c. generator

For the generator design of Table 5, the radial flux density produced by the superconducting field winding at the armature in the presence of an iron environmental screen was computed by GFUN[27] with account being taken of environmental screen length, and the length, depth and slotting arrangement of the superconducting field winding. The computed radial flux density variations are shown as a function of angular position and axial position in Figs. 11 and 12, respectively.

Analysis of the variations in radial flux density with tangential position at the armature radius indicates a maximum harmonic content at the axial centre of the machine of under 1%. Hence the e.m.f. induced in a phase can be assumed to be due to the fundamental harmonic only and is given by

$$E = \frac{r_s \omega k_b Z 2}{\sqrt{2}a} \int_0^l \hat{B}_r(z) \cos \frac{\pi z}{2l} \, dz \text{ volts} \qquad (10)$$

where the variation of radial flux density with axial position $\hat{B}_r(z)$ is shown in Fig. 12.

Computation of the e.m.f. requires numerical integration of the axial variation of radial flux density produced by the field winding, $\hat{B}_r(z)$, while the length and diameter of the helical winding determines the machine inductances

Table 9: Self-inductance values, measured and computed, for model helical winding

	Self-Inductance, μH							
	ex-core				in core			
	measured		computed		measured		computed	
	direct	derived	$\sigma = 15°$	$\sigma = 7{\cdot}5°$	direct	derived	$\sigma = 15°$	$\sigma = 7{\cdot}5°$
Helical turn	0·8		0·71	0·855	0·892		0·827	0·974
30° phasegroup	2·36	2·34	2·26	2·51	2·67	2·64	2·71	2·96
60° phasegroup	6·68	6·65	6·72	7·17	7·64	7·55	8·24	8·70
60° phase L_a	15·1	14·7	14·6	15·5	20·0	19·6	19·6	20·5
phase mutual M_a	4·08	4·08	4·44	4·38	6·12	6·12	6·60	6·53
Synchronous inductance L_s	19·1	19·1	19·0	19·8	26·1	25·7	26·2	27·1
Synchronous inductance (fundamental approx., 60° phasespread)			18·8*	18·9**			25·9*	26·1**

Notes: * This is equivalent to $\sigma = 60°$, identical to vectorially adding 4 e.m.f.s with $\sigma = 15°$, separated by 15°
** Vectorial addition of 4 e.m.f.s with $\sigma = 7{\cdot}5°$, separated by 15°

through eqns. 4 and 6. For a correct design, at a preselected terminal voltage and current, the two quantities of induced voltage and synchronous reactance will satisfy the general phasor diagram shown in Fig. 13.

To design an armature winding, the generator dimensions, reactances and electric and magnetic loadings are obtained using an iterative design technique[8] which assumes the generator windings to be infinitely long and to be represented by fundamental harmonic current sheets at their respective geometric mean winding radii; this reduces the magnetic field problem to two dimensions. A field-winding length is then selected and a flux plot such as that shown in Fig. 12 obtained for the three-dimensional generator configuration. An iterative computer program then computes the induced e.m.f. using numerical integration of eqn. 10 and an estimate of the induced e.m.f. E^* is obtained from the phasor diagram as

$$E^* = \sqrt{1 + 2x_s \sin\phi + x_s^2} \text{ p.u.} \quad (11)$$

For a correct design the e.m.f. E and its estimate E^* must be equal. If E and E^* are not comparable, then armature length and/or the number of armature conductors are varied until a solution is obtained and the subtransient reactance obtained by eqn. 6 is equal to, or greater than, the value computed in the two-dimensional design. This ensures that outer rotor stresses during a short circuit are acceptable. If varying both armature length and the number of conductors will not yield a satisfactory solution, then the length of the rotor field winding must be changed and the iteration repeated.

For an armature of given length the helical winding has been shown to have a lower synchronous reactance (higher short-circuit ratio) than that predicted by two-dimensional analysis for a section of an infinite straight winding of the same length. Hence armature reaction effects are reduced with an helical winding.

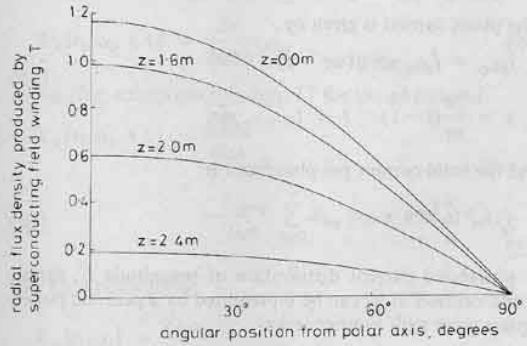

Fig. 11 *Circumferential variation of radial component of flux density produced by superconducting field winding at $r_s = 1{\cdot}0$ m as computed by GFUN at 100% excitation*

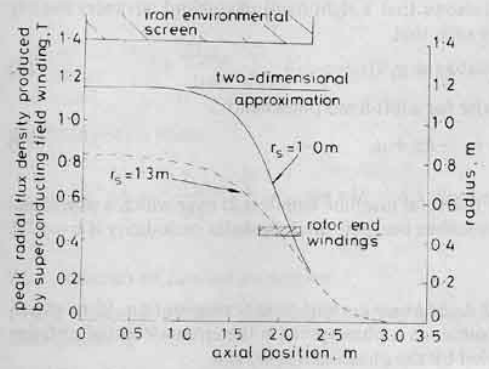

Fig. 12 *Graph showing axial variation of radial component of flux density produced by superconducting field winding (as computed by GFUN at 100% excitation) with relative position of rotor-end windings and environmental screen shown to scale*

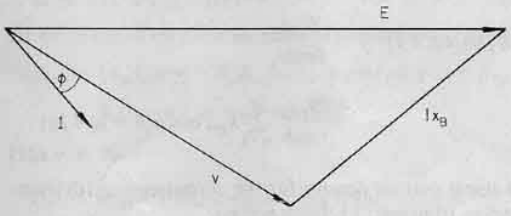

Fig. 13 *Phasor diagram for superconducting a.c. generator*

8 Conclusion

A closed analytical solution has been presented for the magnetic field distribution and machine reactances of a superconducting a.c. machine with an helical armature winding. There is a significant harmonic content in the phasegroup and the phase inductances, but when all three phases are combined to give the synchronous, subtransient and transient inductances many of the harmonics cancel, except those of order $n = 2\tau m \pm 1$, where m is the number of phases and τ any positive integer. Hence the important synchronous, subtransient and transient inductances are largely dominated by the fundamental and therefore can be readily calculated. The reactances can be expressed in a similar form to those for a section of an infinite straight winding, but are modified by two factors, namely a skew factor k_{sn}^2 and an environmental screen factor k_{rn}, both of which contain Bessel functions that depend on the ratio of length to diameter ($k_{sn}^2 = 1$ for a straight winding). Laboratory measurements on a model helical winding indicate that the synchronous reactance expressions are accurate to within 2%.

9 Acknowledgments

The authors would like to thank IRD Co. Ltd., and NEI Parsons Ltd., for permission to publish this paper. They thank their former colleagues in the Electrical Engineering Department of IRD Co. Ltd. for their help and advice and in particular J.S.H. Ross and M. Reay.

The authors would also like to thank Professor P.J. Lawrenson of the University of Leeds for making available the facilities for the model winding measurements and Dr. T.J.E. Miller, formerly of the University of Leeds, who initially designed the model helical winding.

The assistance of C.W. Trowbridge and J. Simpkin of the Rutherford Laboratory in producing Figs. 11 and 12 is gratefully acknowledged.

B.I. Hassall is much indebted to the Science Research Council for financial support.

10 References

1 VICKERS, V.J.: 'Recent trends in turbogenerators', *Proc. IEE*, 1974, **121**, (11R), pp. 1273–1306
2 STEEL, J.G.: 'New designs of large generators', *Engineering*, 1978, **218**, pp. 43–45
3 HORSLEY, W.D.: 'The high speed generator – Eighty years of progress'. 29th Parsons Memorial Lecture, 1964
4 DAVIES, E.J.: 'Airgap windings for large turbogenerator', *Proc. IEE*, 1971, **118**, (3/4), pp. 529–535
5 SPOONER, E.: 'Fully slotless turbogenerators', *ibid.*, 1973, **120** (12), pp. 1507–1520
6 APPLETON, A.D., and ANDERSON, A.F.: 'A review of the critical aspects of superconducting generators'. Presented at the Applied Superconductivity Conference Annapolis, 1972, Paper M2
7 ROSS, J.S.H., ANDERSON, A.F., and APPLETON, A.D.: 'A discussion on large superconducting a.c. generators'. Presented at the International Conference on Electrical Machines, London, 1974, Paper A3
8 ROSS, J.S.H.: 'The engineering design of large superconducting generators'. *ibid.*, Vienna, 1976
9 APPLETON, A.D., ROSS, J.S.H., MITCHAM, A.J., and BUMBY, J.R.: 'Superconducting a.c. generators: Progress on the design of a 1300 MW, 3000 r/min generator'. Presented at the Applied Superconductivity Conference, San Francisco, 1976
10 ROSS, J.S.H., ANDERSON, A.F., and MACNAB, R.B.: 'Alternating Current dynamo-electric machine winding'. British Patent 1395152, 1975
11 ANDERSON, A.F.: Discussion on 'Fully slotless turbogenerators', *Proc. IEE*, 1975, **122**, (1), pp. 75–79
12 FRITSCHE: British Patent 13080, 1887
13 *The Electrician*, April 12, 1889, pp. 655–657
14 SWAINTON, R.: *Des. Eng.*, Feb. 1972, pp. 40–42
15 EASTHAM, J.F., and LAITHWAITE, E.R.: 'Linear motor topology', *Proc. IEE*, 1973, **120**, (3), pp. 337–343
16 EASTHAM, J.F., and ALWASH, J.H.: 'Transverse-flux tubular motors', *ibid.*, 1972, **119**, (12), pp. 1709–1718
17 WATANABE, M., TAKAHASHI, M., TAKAHASHI, N., and TSUKUI, T.: 'Experimental study of a practical airgap winding stator arrangement for large turbine generators'. IEEE Winter Meeting, New York, 1979, Paper F 79 190–0
18 CONLEY, P.L., KIRTLEY, J.L., HAGMAN, W.H., and ULA, A.H.M.S.: 'Demonstration of a helical armature for a superconducting generator'. IEEE PES Summer Meeting, Vancouver, 1979, Paper F79 716–2
19 TAVNER, P.J., PENMAN, J., STOLL, R.L., and LORCH, H.O.: 'Influence of winding design on the axial flux in laminated-stator cores', *Proc. IEE*, 1978, **125**, (10), pp. 948–956
20 EL-MARKABI, M.H.S., and FREEMAN, E.M.: 'The electromagnetic field and shielding of a three phase helical winding placed coaxially inside a multi region cylindrical conducting structure'. Presented at the International Conference on Electrical Machines, Brussels, 1978, Paper G1
21 HAMMOND, P.: 'The calculation of the magnetic field of rotating machines. Part 1 – The field of a tubular current', *Proc. IEE*, 1959, **106**, Part C, pp. 158–164
22 SOUTHALL, H.L., and OBERLY, C.E.: 'System considerations for airborne, high power superconducting generators', *IEEE Trans.*, 1979, **M-15**, pp. 711–714
23 HUGHES, A., and MILLER, T.J.E.: 'Analysis of fields and inductances in air-cored and iron-cored synchronous machines', *Proc. IEE*, 1977, **124**, (2), pp. 121–126
24 BRATOLJIC, T., FURSICH, J., and LORENZEN, H.W.: 'Transient and small perturbation behaviour of superconducting turbo-generators', *IEEE Trans.*, 1977, **PAS-96**, pp. 1418–1429
25 MILLER, T.J.E., and HUGHES, A.: 'Comparative design and performance analysis of air-cored and iron-cored synchronous machines', *Proc. IEE*, 1977, **124**, (2), pp. 127–132
26 MILLER, T.J.E.: 'Transient magnetic fields in the superconducting Alternator'. Ph.D. Thesis, University of Leeds, 1977
27 ARMSTRONG, A.G.A.M., COLLIE, C.J., DISERENS, N.J., NEWMAN, M.J., SIMPKIN, J., and TROWBRIDGE, C.W.: 'New developments in the magnet design computer program GFUN'. Presented at the 5th International Conference on Magnet Technology, Frascati, Rome, 1975
28 ALWASH, S.R.: 'Theoretical and experimental determination of the electrical parameters of a superconducting a.c. generator'. Ph.D. Thesis, University of Leeds, 1980

11 Appendixes

11.1 Linear current density distribution

11.1.1 Notation: The total linear current-density distribution of a phaseband in terms of its axial and tangential linear current density components is

$$K[r_i, \alpha_i, \pm 1] = K_\theta[r_i, \alpha_i, \pm 1]\, a_\theta + k_z[r_i, \alpha_i, \pm 1]\, a_z \tag{12}$$

while the linear current density distribution of a phase-group, with phasebands on different radii is

$$K_g[r_{i,j}, \alpha_i] = K[r_i, \alpha_i, +1] + K[r_j, \alpha_i + \pi, -1] \tag{13}$$

For a phasegroup centred at $\alpha_i + \pi$, the current flow is normally reversed such that the linear current density distribution of a phase is

$$K_{ph}[r_{i,j}, \alpha_i] = K_g[r_{i,j}, \alpha_i] - K_g[r_{i,j}, \alpha_i + \pi] \tag{14}$$

The phase current is given by

$$i_{phq} = \hat{I}_{phq} \sin q(wt - x)$$
$$x = \frac{2\pi}{m}(i-1), \quad i = 1, \ldots, m \tag{15}$$

and the total current per phaseband is

$$i_q = \frac{Z}{b}\frac{i_{phq}}{a} \tag{16}$$

A phaseband current distribution of magnitude $\hat{K}$, spread σ and centred at ϕ_i can be represented by a periodic pulsed square wave with Fourier series

$$f(\theta) = \frac{\hat{K}\sigma}{2\pi} + \sum_{n=1}^{\infty} \frac{2\hat{K}}{n\pi} \sin\left(\frac{n\sigma}{2}\right) \cos n(\theta - \phi_i) \tag{17}$$

Fig. 3 shows that a right-hand phaseband advances linearly with θ such that

$$\phi_i = kz + \alpha_i \tag{18}$$

Likewise for a left-hand phaseband

$$\phi_i = -kz + \alpha_i \tag{19}$$

Since the total machine length is $2l$ over which a phaseband circumscribes one pole pitch the helix periodicity is $k = \pi/2l$.

11.1.2 Axial linear current-density distribution: If the phase-band subtends a phasespread σ the circumferential distance occupied by the phaseband is σr_i and

$$\hat{K}_z[r_i, \alpha_i, \pm 1] = \pm \frac{1}{\sigma r_i}\frac{Z}{ab} i_{phq} \tag{20}$$

Substituting in eqn. 17 and for $f(\theta)$

$$K_z[r_i, \alpha_i, \pm 1] = \pm \frac{Z i_{phq}}{2\pi a b r_i} \pm \frac{Z i_{phq}}{r_i \pi a b} \sum_{n=1}^{\infty} k_{bn} \cos n(\theta - \alpha_i \mp kz) \tag{21}$$

The linear current density for the corresponding ith phase-group is, from eqn. 13, (with $r_i = r_j$)

$$K_{zg}[r_i, \alpha_i] = \frac{2Zi_{phq}}{ab\pi r_i} \sum_{\substack{n=1 \\ n\ \text{odd}}}^{\infty} k_{bn} \cos n(\theta - \alpha_i) \cos nkz + \frac{2Zi_{phq}}{ab\pi r_i} \sum_{\substack{n=2 \\ n\ \text{even}}}^{\infty} k_{bn} \sin n(\theta - \alpha_i) \sin nkz \quad (22)$$

with the corresponding phase value

$$K_{zph}[r_i, \alpha_i] = \frac{4Zi_{phq}}{ab\pi r_i} \sum_{\substack{n=1 \\ n\ \text{odd}}}^{\infty} k_{bn} \cos n(\theta - \alpha_i) \cos nkz \quad (23)$$

11.1.3 Tangential linear current density distribution: Tangential linear current density is again a pulse wave advancing in the z-direction for increasing θ, i.e. $\phi_i = \pm kz + \alpha_i$, with wave period $4l$. The phasespread is $2l\sigma/\pi$ implying

$$\hat{K}_\theta[r_i, \alpha_i, \pm 1] = \frac{Z\pi}{2lab\sigma} i_{phq} \quad (24)$$

giving after substitution in eqn. 17 for the phaseband

$$K_\theta[r_i, \alpha_i, \pm 1] = \frac{Zi_{phq}}{4lab} + \frac{Zi_{phq}}{2lab} \sum_{n=1}^{\infty} k_{bn} \cos n(\theta - \alpha_i \mp kz) \quad (25)$$

and for a phasegroup

$$K_\theta[r_i, \alpha_i] = \frac{Zi_{phq}}{2lab} + \frac{Zi_{phq}}{lab} \sum_{\substack{n=1 \\ n\ \text{odd}}}^{\infty} k_{bn} \sin n(\theta - \alpha_i) \sin nkz + \frac{Zi_{phq}}{lab} \sum_{\substack{n=2 \\ n\ \text{even}}}^{\infty} k_{bn} \cos n(\theta - \alpha_i) \cos nkz \quad (26)$$

and finally for a phase

$$K_{ph}[\alpha_i, r_i] = \frac{2Zi_{phq}}{lab} \sum_{\substack{n=1 \\ n\ \text{odd}}}^{\infty} k_{bn} \sin n(\theta - \alpha_i) \sin nkz \quad (27)$$

11.2 Solution of Laplace's equation

11.2.1 Winding in air: Laplace's equation in cylindrical co-ordinates is

$$\frac{\partial^2\Omega}{\partial r^2} + \frac{1}{r}\frac{\partial\Omega}{\partial r} + \frac{1}{r^2}\frac{\partial^2\Omega}{\partial\theta^2} + \frac{\partial^2\Omega}{\partial z^2} = 0 \quad (28)$$

A solution of the form

$$\Omega = F_1(r)F_2(\theta)F_3(z) \quad (29)$$

can be obtained by the separation of variables such that

$$\Omega_\mu = \{A_\mu I_\mu(\nu r) + B_\mu K_\mu(\nu r)\}\{C_1 \cos(\mu\theta + \nu z + \psi_{1\mu}) + C_2 \cos(\mu\theta - \nu z + \psi_{2\mu})\}$$

$$\mu, \nu \neq 0 \quad (30a)$$

$$\Omega_0 = (A_{01}\theta + A_{02})(A_{03}z + A_{04})(A_{05} + A_{06} \ln(r)),$$

$$\mu = \nu = 0 \quad (30b)$$

Introducing the boundary conditions of Section 11.3 gives

(*a*) inside the winding

$$\Omega_n = A_n I_n(nkr) \begin{cases} \cos[n(\theta - kz) + \psi_{2n}] & \text{r.h. helix} \\ \cos[n(\theta + kz) + \psi_{1n}] & \text{l.h. helix} \end{cases} \quad (31a)$$

$$\Omega_0 = A_{07}z \quad (31b)$$

(*b*) outside the winding

$$\Omega_n = B_n K_n(nkr) \begin{cases} \cos[n(\theta - kz) + \psi_{2n}] & \text{r.h. helix} \\ \cos[n(\theta + kz) + \psi_{1n}] & \text{l.h. helix} \end{cases} \quad (32a)$$

$$\Omega_0 = A_{06}\theta \quad (32b)$$

before the introduction of the environmental screen.

11.2.2 Modification of the potential distribution by the environmental screen: The image winding produces a potential distribution

$$\Omega_n = D_n I_n(nkr) \begin{cases} \cos[n(\theta - kz) + \psi_{2n}] & \text{r.h. helix} \\ \cos[n(\theta + kz) + \psi_{1n}] & \text{l.h. helix} \end{cases} \quad (33)$$

which is incorporated in the potential distributions (eqns. 31 and 32) as,

(*a*) inside the winding

$$\Omega_n = (A_n + D_n) I_n(nkr) \begin{cases} \cos[n(\theta - kz) + \psi_{2n}] \\ \cos[n(\theta + kz) + \psi_{1n}] \end{cases} \quad (34a)$$

$$\Omega_0 = A_{07}z \quad (34b)$$

(*b*) outside the winding

$$\Omega_n = [B_n K_n(nkr) + D_n I_n(nkr)] \begin{cases} \cos[n(\theta - kz) + \psi_{2n}] \\ \cos[n(\theta + kz) + \psi_{1n}] \end{cases} \quad (35a)$$

$$\Omega_0 = A_{06}\theta \quad (35b)$$

D_n is determined by the boundary condition (iv), Section 11.3, and describes the type of environmental screen used.

11.2.3 Magnetic field distributions: The separate components are obtained from $\boldsymbol{H} = -\nabla\Omega$ to give:

(i) Radial fields

$r \leqslant r_s$

$$H_{rn} = -[A_n + D_n] I_n'(nkr) \begin{cases} \cos[n(\theta - kz) + \psi_{2n}] \\ \cos[n(\theta + kz) + \psi_{1n}] \end{cases} \quad (36)$$

$r_x \geqslant r \geqslant r_s$

$$H_{rn} = -[B_n K_n'(nkr) + D_n I_n'(nkr)] \begin{cases} \cos[n(\theta - kz) + \psi_{2n}] \\ \cos[n(\theta + kz) + \psi_{1n}] \end{cases} \quad (37)$$

(ii) Tangential fields

$r \leqslant r_s$

$$H_{\theta n} = [A_n + D_n] I_n(nkr) \frac{n}{r} \begin{cases} \sin[n(\theta - kz) + \psi_{2n}] \\ \sin[n(\theta + kz) + \psi_{1n}] \end{cases} \quad (38)$$

$$r_x \geqslant r \geqslant r_s$$

$$H_{\theta n} =$$

$$[B_n K_n(nkr) + D_n I_n(nkr)] \frac{n}{r} \begin{cases} \sin [n(\theta - kz) + \psi_{2n}] \\ \sin [n(\theta + kz) + \psi_{1n}] \end{cases} \quad (39a)$$

$$H_{\theta 0} = -\frac{A_{06}}{r} \quad (39b)$$

(iii) Axial fields

$$r \leqslant r_s$$

$$H_{zn} = -[A_n + D_n] I_n(nkr) nk \begin{cases} \sin [n(\theta - kz) + \psi_{2n}] \\ -\sin [n(\theta + kz) + \psi_{1n}] \end{cases} \quad (40a)$$

$$H_{z0} = -A_{07} \quad (40b)$$

$$r_x \geqslant r \geqslant r_s$$

$$H_{zn} =$$

$$-[D_n I_n(nkr) + B_n K_n(nkr)] nk \begin{cases} \sin [n(\theta - kz) + \psi_{2n}] \\ -\sin [n(\theta + kz) + \psi_{1n}] \end{cases} \quad (41)$$

where

$$I'_n(nkr) = \frac{\mathrm{d}}{\mathrm{d}r}[I_n(nkr)] = nk\left[I_{n-1}(nkr) - \frac{nI_n(nkr)}{nkr}\right] \quad (42a)$$

$$K'_n(nkr) = \frac{\mathrm{d}}{\mathrm{d}r}[k_n(nkr)] = -nk\left[K_{n-1}(nkr) + \frac{nK_n(nkr)}{nkr}\right] \quad (42b)$$

Substitution of the boundary conditions of Section 11.3 gives

$$A_n = \gamma_n(nkr_i) B_n \quad (43a)$$

$$\psi_{2n} = \psi_{1n} = -n\alpha_i + \pi/2 \quad (43b)$$

$$A_{06} = \mp \frac{Zi_{phq}}{2\pi ab} \quad (43c)$$

$$A_{07} = -\frac{Zi_{phq}}{4lab} \quad (43d)$$

$$B_n[r_i, \alpha_i, \pm 1] = \frac{\pm Zk_{bn} i_{phq}}{n\pi ab[K_n(nkr_i) - \gamma_n(nkr_i) I_n(nkr_i)]} \quad (43e)$$

where

$$\gamma_n(nkr_i) = \frac{K'_n(nkr_i)}{I'_n(nkr_i)} \quad (43f)$$

For an iron environmental screen

$$D_n = -\beta_n(nkr_x) B_n[r_i, \alpha_i, \pm 1] \quad (44a)$$

and

$$\beta_n(nkr_x) = \frac{K_n(nkr_x)}{I_n(nkr_x)} \quad (44b)$$

and for a conducting environmental screen

$$D_n = -\gamma_n(nkr_x) B_n[r_i, \alpha_i, \pm 1] \quad (45a)$$

and for no environmental screen

$$D_n = 0 \quad (45b)$$

Substitution of these constants with the magnetic-field expressions, eqns. 36 to 42, gives the magnetic field distributions for an individual phaseband listed in Table 1. Corresponding linear current-density distributions are also shown in this Table. Magnetic-field distributions for a phasegroup, phase and total machine phases can now be obtained by progressive use of superposition; the first stage, that of combining phasebands to form a phasegroup being shown in Table 3. Table 2 defines the environmental screen factors used in Tables 1 and 3.

11.3 Boundary conditions

(i) By comparison with the linear current density distributions of Section 11.1 for periodicity in θ and z

$$\mu = n$$

the space harmonic number and

$$\nu = nk = \frac{\pi n}{2l}$$

for a right-hand helixed winding

$$C_1 = 0, \quad C_2 = 1$$

for a left-hand helixed winding

$$C_1 = 1, \quad C_2 = 0$$

(ii) As $r \to 0$, $K_n(nkr) \to \infty$ while the magnetic fields are finite.

$$B_n = 0 \quad \text{for} \quad r < r_i.$$

(iii) For a helical winding in air (no environmental screen) as $r \to \infty$, $I_n(nkr) \to \infty$ while the magnetic fields tend to zero. $A_n = 0$ for $r > r_i$.

(iv) The boundary conditions at the environmental screen depend on the type of screen:

(*a*) No environmental screen. In this case no image winding is necessary and the previous boundary conditions are sufficient.

(*b*) Iron environmental screen. ($\mu_r = \infty$, $\rho = \infty$). All the flux enters the iron core normally such that at $r = r_x$, $H_\theta = H_z = 0$.

(*c*) Conducting environmental screen ($\mu_r = 1$, $\rho = 0$). All the flux is excluded from the environmental screen such that at $r = r_x$, $H_r = 0$ for all θ and z.

(*d*) At the stator current sheet radial flux density is continuous and

$$H_{\theta n_{\text{outside}}} - H_{\theta n_{\text{inside}}} = K_{zn}$$

$$H_{zn_{\text{outside}}} - H_{zn_{\text{inside}}} = -K_{\theta n}$$

11.4 Inductance calculations

11.4.1 Phasegroup inductances: The total flux entering the Gaussian surface of Fig. 5 from a phasegroup of Z/b turns centred at $\theta = \alpha$ is

$$\phi_{gn}(\alpha) = \mu_0 \int_{-l}^{+l} \int_{kz}^{\pi - kz} -H_{rgn}[r_s, \alpha] r_s \mathrm{d}\theta \mathrm{d}z + \mu_0 \int_{0}^{r_s} \int_{-\pi}^{\pi} H_{zgn}[r_s, \alpha] r \mathrm{d}\theta \mathrm{d}r \quad (46)$$

Evaluating this integral and replacing the first helical loop by a phasegroup of Z/b turns and breadth factor k_{bn} gives the mutual flux linkage between phasegroups as

$$\Phi_{g0}(\alpha) = \frac{\mu_0 Z^2 \pi r_s^2}{2ab^2 l} i_{ph} \tag{47}$$

$$\Phi_{gn}(\alpha) = \frac{2\mu_0 r_s Z^2 k_{bn}^2 k_{sn}^2 k_{rn}}{nkr_s ab^2} i_{ph} \cos n\alpha$$

where k_{sn}^2 is defined as the skew factor, and

$$k_{sn}^2 = -\frac{\gamma_n(nkr_s)[kr_s I_{n-1}(nkr_s) - I_n(nkr_s)]}{[K_n(nkr_s) - \gamma_n(nkr_s) I_n(nkr_s)]} \tag{48}$$

k_{rn} is the radial flux environmental screen factor defined in Table 2, column 1. Mutual inductance is obtained from

$$M_{gn}(\alpha) = \frac{\Phi_{gn}(\alpha)}{i_{ph}/a} \tag{49}$$

giving

$$M_{g0}(\alpha) = \frac{\mu_0 Z^2 \pi r_s^2}{2b^2 l} \quad \text{H} \tag{50}$$

$$M_{gn}(\alpha) = \frac{2\mu_0 Z^2 k_{bn}^2 k_{sn}^2 k_{rn} 2l}{\pi n b^2} \cos n\alpha \quad \text{H}$$

for all n

the total mutual inductance being the sum of the harmonic components

$$M_g(\alpha) = M_{g0}(\alpha) + \sum_{n=1}^{\infty} M_{gn}(\alpha) \tag{51}$$

11.4.2 Phase inductance: Phasegroups may be interconnected in a variety of ways to produce a phase, the most usual being:

(i) a phase and phasegroup are identical

(ii) two phasegroups 180° phase displaced are connected in parallel

(iii) two phasegroups 180° phase displaced are connected in series to give

$$M_{phn}(\alpha) = \frac{b^2}{4a^2} M_{gn}(\alpha) \tag{52}$$

$$M_{phn}(\alpha) = \frac{\mu_0 Z^2 k_{bn}^2 k_{sn}^2 k_{rn} 2l}{2\pi n a^2} \cos n\alpha \quad \text{H} \tag{53}$$

n odd

11.4.3 Synchronous inductance: For an m-phase generator with no saliency the synchronous inductance is

$$L_{sn} = \frac{m}{2} M_{phn}(0) \tag{54}$$

$$n = 2\tau m \pm 1$$

τ any integer

giving

$$L_{sn} = \frac{m\mu_0 Z^2 k_{bn}^2 k_{sn}^2 k_{rn} 2l}{4\pi n a^2} \quad \text{H} \tag{55}$$

11.4.4 Subtransient inductance: The image winding representing the outer-rotor screen introduces an additional magnetic scalar potential distribution of the form

$$\Omega_n = F_n K_n(nkr) \begin{cases} \cos[n(\theta - kz) + \psi_{2n}] & \text{r.h. helix} \\ \cos[n(\theta + kz) + \psi_{1n}] & \text{l.h. helix} \end{cases} \tag{56}$$

which combined with eqns. 34 and 35 gives

(*a*) inside the winding

$$\Omega_n = \{[A_n + D_n] I_n(nkr) + F_n K_n(nkr)\} \begin{cases} \cos[n(\theta - kz) + \psi_{2n}] \\ \cos[n(\theta + kz) + \psi_{1n}] \end{cases} \tag{57a}$$

$$\Omega_0 = A_{07} z \tag{57b}$$

(*b*) outside the winding

$$\Omega_n = \{D_n I_n(nkr) + [B_n + F_n] K_n(nkr)\} \begin{cases} \cos[n(\theta - kz) + \psi_{2n}] \\ \cos[n(\theta + kz) + \psi_{1n}] \end{cases} \tag{58a}$$

$$\Omega_0 = A_{06} \theta \tag{58b}$$

Introduction of the additional boundary condition at the outside radius of the outer rotor modifies the scalar magnetic potential and field distributions in such a way that the environmental screen factors $k_{\theta n}$, k_{zn} and k_{rn} of Table 2 are modified to those of Table 4. Consequently, with an iron environmental screen the radial field outside the stator winding is given by

$$H_{r_s n} = \pm \frac{Z k_{bn} i_{ph}}{n\pi ab} \frac{K_n'(nkr_s)}{[K_n(nkr_s) - \gamma_n(nkr_s) I_n(nkr_s)]} \times \frac{\left[1 - \frac{\beta_n(nkr_x)}{\gamma_n(nkr_s)}\right]\left[1 - \frac{\gamma_n(nkr_s)}{\gamma_n(nkr_D)}\right]}{\left[1 - \frac{\beta_n(nkr_x)}{\gamma_n(nkr_D)}\right]} \sin n(\theta - \alpha_i \mp kz) \tag{59}$$

For nonzero n there is no net axial flux entering the Gaussian surface of Fig. 5 and so the phase inductances are entirely due to radial magnetic fields and the subtransient inductance is

$$L_{dn}'' = \frac{m\mu_0 Z^2 k_{wn}^2 k_{rn} 2l}{4\pi n a^2} \frac{\left[1 - \frac{\gamma_n(nkr_s)}{\gamma_n(nkr_D)}\right]}{\left[1 - \frac{\beta_n(nkr_x)}{\gamma_n(nkr_D)}\right]} \tag{60}$$

A.F. Anderson was born in Edinburgh, Scotland, in July 1939. He received a first class honours degree in Electrical Engineering and the Ph.D. degree from the University of St. Andrews in 1962 and 1966, respectively.

From 1965 to 1967 he worked as an application engineer on rolling-mill drives with the Plant Application Engineering Department AEI Ltd., Rugby. From 1967 to 1970 he was an NRDC Post Doctoral Fellow at the University of Dundee working on axially laminated reluctance motors. In 1970 he joined the Electrical Engineering Department of International Research and Development Co. Ltd., where he worked on superconducting a.c. generators and on timing motors. In 1971 he was appointed Group Leader of the superconducting a.c. machines Group.

In 1974 he joined the Electromagnetics Group of the Electrical Research Department of C.A. Parsons Ltd., Newcastle, and in 1976 he was appointed Group Leader, with responsibilities for the instrumentation of large machines and experimental investigation into their electromagnetic behaviour under service conditions.

Dr. Anderson is a Member of the Institution of Electrical Engineers.

J.R. Bumby was born in Thirsk, England, in April 1949. He received a first class honours degree in Engineering Science and the Ph.D. degree in Electrical Engineering from the University of Durham, in 1970 and 1974, respectively.

He joined the Electrical Engineering Department of International Research & Development Co. Ltd., Newcastle-upon-Tyne, in 1973 where he worked on superconducting a.c. generators, hybrid electric vehicles and the generation of electrical energy from sea-wave energy. In 1975 he was made responsible for the electrical design of superconducting a.c. generators and in 1977 he was appointed Group Leader of the Special Electrical Projects.

In 1978 he joined the Department of Engineering Science, University of Durham as a lecturer in Electrical Engineering. Dr. Bumby's current research interests are superconducting machines and power system stability and control.

Dr. Bumby is an Associate Member of the Institution of Electrical Engineers.

B.I. Hassall graduated in 1975 from Nottingham University with first class honours in Electrical and Electronic Engineering. He was then appointed Research Officer at International Research and Development Co. Ltd., Newcastle-upon-Tyne to work on superconducting a.c. generators. In January 1978 he became a Research Fellow at Leeds University under part of the SRC's programme investigating a.c. generators.

Mr. Hassall is an Associate Member of the Institution of Electrical Engineers.

A.F. Anderson was born in Edinburgh, Scotland, in July 1939. He received a first class honours degree in Electrical Engineering and the Ph.D. degree from the University of St. Andrews in 1962 and 1966, respectively.

From 1965 to 1967 he worked as an application engineer on rolling-mill drives with the Plant Application Engineering Department AEI Ltd., Rugby. From 1967 to 1970 he was an NRDC Post Doctoral Fellow at the University of Dundee working on axially laminated reluctance motors. In 1970 he joined the Electrical Engineering Department of International Research and Development Co. Ltd., where he worked on superconducting a.c. generators and on timing motors. In 1971 he was appointed Group Leader of the superconducting a.c. machines Group.

In 1974 he joined the Electromagnetics Group of the Electrical Research Department of C.A. Parsons Ltd., Newcastle, and in 1976 he was appointed Group Leader, with responsibilities for the instrumentation of large machines and experimental investigation into their electromagnetic behaviour under service conditions.

Dr. Anderson is a Member of the Institution of Electrical Engineers.

J.R. Bumby was born in Thirsk, England, in April 1949. He received a first class honours degree in Engineering Science and the Ph.D. degree in Electrical Engineering from the University of Durham, in 1970 and 1974, respectively.

He joined the Electrical Engineering Department of International Research & Development Co. Ltd., Newcastle-upon-Tyne, in 1973 where he worked on superconducting a.c. generators, hybrid electric vehicles and the generation of electrical energy from sea-wave energy. In 1975 he was made responsible for the electrical design of superconducting a.c. generators and in 1977 he was appointed Group Leader of the Special Electrical Projects.

In 1978 he joined the Department of Engineering Science, University of Durham as a lecturer in Electrical Engineering. Dr. Bumby's current research interests are superconducting machines and power system stability and control.

Dr. Bumby is an Associate Member of the Institution of Electrical Engineers.

B.I. Hassall graduated in 1975 from Nottingham University with first class honours in Electrical and Electronic Engineering. He was then appointed Research Officer at International Research and Development Co. Ltd., Newcastle-upon-Tyne to work on superconducting a.c. generators. In January 1978 he became a Research Fellow at Leeds University under part of the SRC's programme investigating a.c. generators.

Mr. Hassall is an Associate Member of the Institution of Electrical Engineers.